9950-801

THREE DIMENSIONAL RAY TRACING OF THE JOVIAN MAGNETOSPHERE IN THE LOW FREQUENCY RANGE

SwRI Project No. 15-6546
JPL Contract No. 956026

Final Report

October 1982

J. D. Menietti
Southwest Research Institute
P. O. Drawer 28510
San Antonio, TX 78284

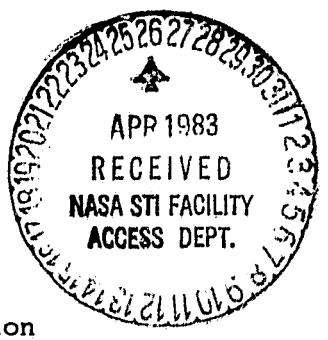

This work was performed for the Jet Propulsion Laboratory, California Institute of Technology sponsored by the National Aeronautics and Space Administration under Contract NAS7-100.

ABSTRACT

Ray tracing of the Jovian magnetosphere in the low frequency range (1-40 MHz) has resulted in a new understanding of the source mechanism for Io dependent decametric radiation (DAM). Our three-dimensional ray-tracing computer code has provided model DAM arcs at 10° intervals of Io longitude source positions for the full 360° of Jovian system III longitude. In addition, particularly interesting arcs have been singled out for detailed study and modelling. The results of this study indicate that DAM arcs may be categorized according to curvature--the higher curvature arcs are apparently due to wave stimulation at a non-constant wave normal angle, ψ. The $\psi(f)$ relationship has a signature that may be common to most of the higher curvature arcs. The low-curvature arcs, on the other hand, seem to be adequately modelled with a constant wave normal angle of close to 90°. These results imply that for higher-curvature arcs observed far from Jupiter (to diminish spacecraft motion effects) the electrons providing the gyro-emission may be relativistically beamed.

TABLE OF CONTENTS

INTRODUCTION

One of the most characteristic features of the Jovian high frequency radio emissions is the presence of the arc-like structures in frequency-time spectrograms. These emissions have been observed in the decameter (DAM) frequency range of 1 MHz to 40 MHz and the arcs occur as single-valued and double-valued in frequency and as a series of closely-spaced (nested arcs in time (see Figs. 1 and 2). Careful study has disclosed the arc-like structures even on ground-based spectrograms (Boischot et al., 1981).

The radiation is observed both in the right and left hand optical polarizations as if coming from source regions in the northern and southern hemispheres. Boischot and Lecacheaux (1981) have noted a remarkable repeatability of features at certain Io phases. The arcs can be described as being vertex-early or vertex-late if the "nose frequency" occurs at earlier or later Jovian longitudes respectively. In addition the arcs are labelled as "great arcs" if their frequency extent is $\lesssim$5 MHz to $\gtrsim$20 MHz. Sources are described as being either A, B, C, or D if arcs are observed in the following Jovian system III longitude ranges: source A or main source (190° < CML < 290°); source B or early source (60° < CML < 190°); source C or late source (290° < CML < 30°); source D (30° < CML < 60°).

A study of the Voyager I and II data shows that many of the nested arcs are not double-valued arcs (double-valued in frequency), but rather a series of small-radius-of-curvature arcs. Total time duration of an individual shallow arc typically ranges from three to thirty minutes. The time interval between nested arcs can be quite small, sometimes less than one minute. The higher-radius-of-curvature arcs are longer in time duration (possibly >2 hrs) and sometimes are nested in groups as well.

Various source mechanisms have been proposed to explain decametric arcs. Many investigators attribute the emissions to precipitating electrons along the Io flux tube which then interact with the Jovian ionosphere and upper atmospheric plasma via a gyro-emission mechanism (cf Neubauer et al. 1980).

The resulting radiation is envisioned as being emitted in a hollow cone of half angle, ψ, with respect to the B-field. Warwick et al., (1981) suggest the arc structure is due to anomalous B-field islands at the base of the Io flux tube. Boischot (1981) suggests an interesting interference effect with the Io torus as the source of the arcs. In this paper we suggest propagation effects through the Jovian ionosphere and magnetosphere as the arc-producing mechanism.

Some preliminary work has been done to describe the growth rate of the earth's AKR emissions, analogous emission to the Jovian DAM radiation (cf. Omidi and Gurnett, 1982; Wu et al 1982; Calvert, 1982). These authors' findings suggest that for conditions as might be expected at the foot of the Io flux tube (i.e. $\omega_p/\omega_g<1$) emission should occur at large ($\gtrsim 60°$) angles with respect to the magnetic field (large wave normal angles).

In this paper three-dimensional ray-tracing of the Jovian DAM radiation is performed using a realistic Jovian plasma model (Sentman and Goertz, 1979), and the O-4 magnetic field model (Acuna and Ness, 1979). The purpose of this paper is to perform three-dimensional ray-tracing of DAM radiation from source positions along an Io flux tube at frequencies close to the right-hand extraordinary (RX) mode cutoff frequency, $f_{RX} = f_g/2 + \sqrt{f_g^2 + f_p^2}$ (f_g = gyrofrequency; f_p = plasma frequency). Jovian arcs are produced with minimal assumptions about the source mechanism. We suggest it is possible to explain

the low-curvature arcs as due to the mechanism of multiple reflections of Alfven waves as presented by Neubauer (1979) and Goertz (1980), and elaborated by Gurnett and Goertz (1981). A constant wave normal angle at each frequency-dependent source point sufficiently reproduces the observed results. We explain the large sometimes isolated high-curvature arcs as due to source points with wave normal angles which vary as a function of frequency in a repeatable fashion, and we suggest these latter arcs are a result of more energetic field-aligned particles than are the low-curvature arcs.

B-field and Plasma Models.

The raypaths calculated by the procedure described above are dependent on the magnetospheric model chosen. The description of the Jovian magnetic field utilized in these calculations (the O-4 model) is that published by Acuna and Ness (1976); the background plasma, Sentman and Goertz (1978); and the Io torus, Warwick, et al (1979). Figure 3 is an abbreviation of this combined "Jovian magnetosphere" showing contours of plasma frequency in the 200° -20° meridian plane. Suspected source regions in the northern and southern hemispheres are shaded. Spherical harmonic expansion coefficients are used to calculate the magnitude of the field B_o, the components B_r, B_θ, and $B\phi$ and their derivatives. The plasma density along the raypath, and the spatial gradients are calculated from empirical fits.

Emission Mechanism

In this study the following assumptions have been made concerning the Jovian emission mechanism:

1. The radiation is in the right-hand polarized extraordinary mode.
2. The source region is at the foot of the Io flux tube and the source mechanism is Doppler-shifted gyroemission.
3. The emission cone is hollow.

Assumption No. 1 is stongly supported by the data set (cf. Warwick et. al.). The strongest emissions are RX, and when left hand polarization is present, the source is most likely the southern hemisphere. For this work the emission mechanism assumed is that first presented by Neubauer, (1979); Goertz, (1980); Gurnett and Goertz, (1980). The mechanism depicts Io interacting with the Jovian magnetosphere and generating large amplitude standing Alfven waves which propagate northward and southward along the magnetic field lines from Io. Each Alfven wave is associated with a pair of oppositely directed currents, in this model, which flow along the Alfven precipitation path between Io and the Jovian ionosphere. Assumption No. 2 is consistent with this picture. The degree of Doppler shifting is one of the subjects of this investigation. Finally, a hollow emission cone for the DAM is strongly suggested by the data (Carr and Gulkis, 1969). Analogously to terrestrial auroral kilometric radiation (AKR) the initial DAM radiation at a given frequency is assumed approximately perpendicular to the magnetic field, i.e., the initial wave normal angle, ϕ, is aproximately 90° (this assumption is later relaxed) . Those rays emanating from a lower Jovian source altitude are closer to the R-X cutoff frequency, and thus are refracted more. While AKR emissions

have filled emission cones, Jovian DAM emissions, whose source points are in regions of much lower density than AKR emissions, are believed to have hollow emission cones. Another important point is that the wave normal angle is a function of frequency. In general the higher frequencies with source points close to the surface have smaller wave normal angles than do lower frequencies with higher altitude source locations.

RESULTS

To calculate propagation ray paths in the Jovian magnetosphere we have used a three-dimensional ray-tracing program. The computer code is based on the Stix cold-plasma formulation of the index of refraction and Haselgrove's set of first order differential equations amenable to numerical solution. Chosen as inputs are: a source position (in radial distance, longitude, and latitude) from which waves at a specific frequency, f, are to be launched at a specific wave normal angle (WNA), ϕ, with respect to the magnetic field. Different frequencies originating from source points on the same field line or on adjacent field lines would generate a set of nested emission cones. Depending on the geometry of these cones, imposed by the plasma and by the B-field, the spacecraft would detect frequencies which decrease or increase with time as these cones sweep over the detector.

At the source region, the program calculates an index of refraction surface for R-X mode waves, based on B-field and on background plasma parameters. Next, the program takes an incremental step in the direction perpendicular to the index of refraction surface, i.e., in the direction of the group velocity or energy flow, and then determines the coordinates of this new point on the raypath. Then, another index of refraction surface is calculated through this

new point and the steps are repeated. The direction of each ray changes according to Snell's law as it travels through the magnetized plasma. To generate an emission cone, thirty-six rays are launched, one every 10° around B at the specified wave normal angle and frequency.

Radiation Sheets of Varying Frequency.

Figures 4 and 5 present mercator projections of certain radial shells centered on Jupiter. The intersections of the calculated, model-dependent emission cones with these radial shells are labeled according to frequency. In Figure 4, the radial shell is at $6R_J$ and the Io torus is shown in shaded cross-section. Jovian latitude is indicated on the vertical axis and longitude System III '65, on the horizontal axis. Each point on the figure is the intersection of a raypath with the $6R_J$ shell. In three dimensions, not shown here, the rays could be visualized as the bent ribs of an umbrella, while the fabric would correspond to the warped emission cone. All of the rays in Figure 4 were launched at $\psi = 90°$. Emission cones of two frequencies, 2 MHz and 20 MHz, originate from source points in the northern hemisphere labeled "X", and emission cones of 2 MHz and 10 MHz radiation originate from source points in the southern hemisphere. At $6R_J$ parts of the emission cones are penetrating the model Io plasma torus with no noticeable effect. In fact, the torus was "invisible" to all DAM frequencies of this study. From close scrutiny of Figure 4, one notices the source points for different frequencies are displaced in longitude (horizontally), as well as in latitude. Since different frequencies are launched near the local gyrofrequency, one expects the source points to have different latitudes. The longitudinal separation of the source points for two frequencies is an indication of the azimuthal twist in the

field line threading Io. This field line is shown dashed, as it is projected onto the $6R_J$ shell. Also, notice that the emission cones of differing frequencies can intersect, and cross over one another. Finally, notice how the emission cones directed toward the southern hemisphere are tilted around the source point and appear to be rotated with respect to the northern hemisphere emission cones.

The trajectory of the raypaths out to a distance of 100 R_J is illustrated in Figure 5. The points represent the same rays seen in Figure 4, but now traced to $100R_J$. Comparing Figure 4 with Figure 5, it is easy to see that the emission cones have spread out. Near longitude 230°, the radiation from the northern hemisphere sources reaches a southern latitude of -60°, while the radiation emanating from the southern sources reaches a northern latitude of 45°. The radiation sheets at $100R_J$ intersect the equatorial plane at different points (more widely separated) compared with the intersections of the same sheets with the equatorial plane at $6R_J$. Notice that the radiation sheets at 100 R_J are smooth and have the same gentle curvature as those at 6 R_J. Since a portion of the emission cones traversed the Io plasma torus at $6R_J$, one might expect "kinks" to occur in the cones, beyond the torus. No evidence of refraction effects, caused by the model torus, are seen in the lower panel. We conclude that the torus has negligible effect even at 2 MHz, the lowest frequency traced, and leads us to surmise that the major propagation effects occur near the source regions.

Closer examination of the projection at $100R_J$ reveals "crossings" of the emission cones of different frequencies. This should not be surprising since different frequencies are launched from different source points, assuming radiation occurs near the local electron gyrofrequency. The twist in the field

lines from one source point to the next produces intersections of the emission cones of different frequencies. The trajectory of Voyager 1 was slightly above the Jovian equator. As the magnetic field rotates, the emission cones sweep from left to right over the spacecraft (or, in the Jovian frame, the spacecraft flies from right to left, slightly above the equator). As the spacecraft intercepts these emission cones, the PRA experiment records frequencies which decrease or increase with time, depending on the nature of these intersections, i.e., the geometry of the emission cones.

Radiation Sheets of Varying Wave Normal Angle

The top panel of Figure 6 contains emission cones for 2 MHz and WNA's of 60°, 80°, 100°, and 120°. Rays with initial WNA >90° (ψ>90°) are initially directed toward the planet. This mercator projection was taken at the 100R_J radial shell. Note that the emission cones "open up" as the WNA increases from 60° to 100°, then the radiation emitted at ψ = 120° refracts upwards away from the R-X cutoff. The bottom panel illustrates the same effect for emission cones of 25 MHz. WNA is one parameter which shifts the intersection of the emission cones at the equator (and at the spacecraft) toward earlier or later longitudes.

Radiation Sheets Emanating from Varying Source Longitudes

Figure 7 shows emission cones of frequency 25 MHz, WNA = 90° at the 100R_J shell. The projected source positions are located at the top of the frame. If adjacent field lines are sources of emission at a given WNA, a family of "nested emission cones" of that particular frequency is produced. The refracting of the emission cones from left to right across the frame may be caused

by the azimuthal assymmetry in the field, which is an integral part of this model. As the Jovian magnetic field rotates, the spacecraft would be illuminated by this frequency as long as these emission cones intersect the spacecraft position. The spacecraft could "fly out of" this emission when sources are absent on adjacent field lines or when the geometry of the emission cones produces no illumination of the spacecraft.

MODEL ARC RESULTS

A typical signature of arc quite common in the data is that of the short time duration, low-curvature nested arcs which can extend over a frequency range of f >30 MHz. (Fig. 2). In order to construct model low curvature arcs the dynamics of the problem were considered: Jupiter was rotating; Io was revolving; and the spacecraft was moving. To minimize the effects of spacecraft motion the ray path emission cone projections were examined at large radial distance (150 R_J). During the time of observation of an arc the central meridian longitude of Jupiter changes. For each change in Io system III longitude of 10°, the spacecraft system III longitude varies by about 13° (when the spacecraft is far from Jupiter). In this study we assume that the Io flux tube is the radiation source. Initially we consider only the case of emission from a series of constant Io longitudes, each successive Io longitude 10° different from the previous. We also initially assume emission at only one wave normal angle, $\psi \approx 90°$. Figure 8 is a plot of frequency versus spacecraft system III (1965) longitude. On the right in this figure curves for three different Io flux tubes are shown: Io longitude = 180°, 190°, and 200°. Each point on each model curve represents the spacecraft longitude at which the chosen frequency intersects the spacecraft latitude at the time of observation. Source points for the seven different frequencies chosen are

located along each Io flux tube at positions just above the R-X cutoff frequency. For all cases where the wave normal angle, ϕ, is approximately 90°, which was the case for the low curvature nested arcs modelled, the Doppler shift was assumed minimal: $f/f_g = 1.005$. This value is just large enough to prevent singularities at the source point in the computer code. The series of model low curvature nested arcs shown (vertex-late in this case) qualitatively matches a series of nested arcs observed by the PRA experiment on Voyager 2 when the spacecraft longitude and Io's longitude were close to those used in the model case . One of the actual arcs is plotted for comparison in Fig. 8. There is a slight discrepancy between the model arcs and the data at the higher frequencies. This discrepancy may be due to emission from slightly smaller wave normal angles at the higher frequencies. For the case of most low curvature nested arcs, the time duration of an arc is so small (several min.) that the Io flux tube longitude of the source can be assumed constant for the duration of the arc. Also shown in Figure 8 are two model vertex-early-nested arcs (quite small curvature in this case) and the observed Voyager 2 arc at the approximate same spacecraft system III longitude and appropriate Io flux tube source longitude. The two model arcs shown bracket the observed arc. The model shows good qualitative agreement with the actual data, but the model Io longitude and actual Io longitude during the time of the observed arc differ by approximately 25°. This discrepancy is probably due to the difference between the magnetic field model (O-4) and the actual magnetic field at low altitudes near the source point.

We have modelled arcs for source longitudes at 10° intervals for the full 360° of System III longitude. The model arcs are all for an assumed Doppler shift frequency ratio of $f/f_g = 1.005$ and $\phi \approx 90°$. To construct the arcs it

was assumed that the spacecraft was at 150 R_J and at a latitude of 3.2°. Again, each point on each model curve represents the spacecraft longitude at which the chosen frequency intersects the approximate spacecraft latitude at the time of observation. Hence each point was determined by intersecting the approximate spacecraft latitude with the model-generated emission cone surface at a radial distance of 150 R_J. The results are shown in Fig. 9. One must be careful not to construe this figure as being what the spacecraft actually observed. Such should be the case only for arcs of slight curvature, i.e., short time duration, otherwise Jovian rotation and Io revolution effects need be taken into account. In Figure 9 only the model arcs of small curvature can be directly compared to the data as explained above. This includes the Io longitudes from approximately 100° to 230° when the spacecraft is in the respective system III longitude range from approximately 60° to 300°. At both high and low Io longitudes the modelled arc signatures change. For some arcs the time duration becomes greater than thirty minutes. For others the curvature becomes quite high. These morphological changes may be due to azimuthal assymmetries in the magnetic field O-4 model. The low curvature arcs occur when the angle, ϕ, at Jupiter between the spacecraft and Io differs only slightly from 90° (by say no more than 20°).

We find that our model of low curvature arcs with $\phi \approx 90°$ agrees reasonably well with the data set--the V2 examples cited in Figure 8 for days 79-182 and 79-197 are typical cases. Low curvature arcs as observed by Voyager 1 on day 79-63 from about 950 to 1030 are shown in Figure 2. At 1005 in this Figure the spacecraft longitude is given as 152° and the Io longitude at the same time is 238°. Referring to Figure 9 we find good agreement between the observed arcs and the model-produced low-curvature arcs at the same approximate spacecraft longitude and Io longitude.

was assumed that the spacecraft was at 150 R_J and at a latitude of 3.2°. Again, each point on each model curve represents the spacecraft longitude at which the chosen frequency intersects the approximate spacecraft latitude at the time of observation. Hence each point was determined by intersecting the approximate spacecraft latitude with the model-generated emission cone surface at a radial distance of 150 R_J. The results are shown in Fig. 9. One must be careful not to construe this figure as being what the spacecraft actually observed. Such should be the case only for arcs of slight curvature, i.e., short time duration, otherwise Jovian rotation and Io revolution effects need be taken into account. In Figure 9 only the model arcs of small curvature can be directly compared to the data as explained above. This includes the Io longitudes from approximately 100° to 230° when the spacecraft is in the respective system III longitude range from approximately 60° to 300°. At both high and low Io longitudes the modelled arc signatures change. For some arcs the time duration becomes greater than thirty minutes. For others the curvature becomes quite high. These morphological changes may be due to azimuthal assymmetries in the magnetic field O-4 model. The low curvature arcs occur when the angle, ϕ, at Jupiter between the spacecraft and Io differs only slightly from 90° (by say no more than 20°).

We find that our model of low curvature arcs with $\phi \approx 90°$ agrees reasonably well with the data set--the V2 examples cited in Figure 8 for days 79-182 and 79-197 are typical cases. Low curvature arcs as observed by Voyager 1 on day 79-63 from about 950 to 1030 are shown in Figure 2. At 1005 in this Figure the spacecraft longitude is given as 152° and the Io longitude at the same time is 238°. Referring to Figure 9 we find good agreement between the observed arcs and the model-produced low-curvature arcs at the same approximate spacecraft longitude and Io longitude.

Our emission mechanism assumes that DAM is the result of Doppler-shifted gyro-emission from accelerated, field-aligned electrons. As noted by Omidi and Gurnett (1982) the condition that must obtain at relativistic gyro-emission resonance (condition for maximum wave growth rate) is

$$\beta = \frac{V_\parallel}{c} = \frac{\omega}{\omega_g} n \cos \psi - \frac{\omega}{\omega_g} n \cos \psi \left[1 - \frac{2(\omega-\omega_g}{\omega_g} \left(\frac{\omega_g}{\omega}\right)^2 \frac{1}{n^2\cos^2\psi}\right]^{1/2} \qquad (1)$$

where "n" is the phase index of refraction and the subscript "g" refers to the gyrofrequency. Solving (1) for $d\psi/df$ yields

$$\frac{d\psi}{df} = \frac{-\omega_g(2 - \beta^2)}{4\pi n \beta \sin \psi f^2} \quad . \qquad (2)$$

This expression suggests that the observed peak in $\psi(f)$ must be explained geometrically since no physical values of the variable parameters will allow $d\psi/df > 0$.

For both cases in Figure 10 the Io flux tube intersects Jupiter at a longitude where little azimuthal assymmetry in the O-4 B-field model is present (particularly so for the V1 example at Io III longitude ≈180° [during arc emission the Io longitude changes by a few degrees]). The results seem to be best explained by noting that since the source positions for the highest frequencies along the Io flux tube are closer to the planet by about 1 R_J, increased refraction of the higher frequencies refracts the emission cones so that the spacecraft observes the higher frequencies "inside" the emission cones of the lower frequencies in a three dimensional ray path.

Further analysis of Equation 1 has allowed us to suggest the most probable value of the Doppler shifting present for the higher-curvature arcs. Goldreich and Lynden-Bell give the ratio f/f_g for the proposed Doppler-shifted gyro-emission as

$$\frac{f}{f_g} \approx 1 + \left(\frac{v_\parallel}{c}\right)^2 \qquad (3)$$

For a reasonable range of values of β, Equation (1) allowed us to set limits on the range of ϕ. Table I contains calculated values of the maximum ϕ for a given β.

TABLE I

β	f/f_g	ϕ_{max}
0.05	1.0025	85.7°
0.1	1.01	81.4°
0.15	1.023	76.95°
0.2	1.04	73.2°
0.25	1.0625	71.9°
0.30	1.09	65.6°

Table I indicates the relativistic beaming effect and strong dependence of ϕ on the ratio, f/f_g, allowed by the resonance condition, equation (1).

Recall that the low curvature arcs in most cases can be modelled adequately for $\phi \approx 90° \approx$constant. The higher-curvature arcs, on the other hand, require smaller wave normal angles by about 15° -20° for typical examples. Hashimoto and Goldstein (1982) have also found from their ray-tracing results that as f/f_g increases, smaller initial values of ϕ ($\approx 70°$) gave better fits to the data. This suggests that the higher-curvature arcs are produced by a more energetic electron field-aligned beam. Our results indicate, for the cases

studied in detail, that $\phi_{max} \lesssim 76°$ indicating that $\beta \approx .16$ or $f/fg \approx 1.02$. The low curvature arcs require little or no beaming to explain their flat (low-curvature) signatures. While we can say little about the low curvature arc electron energies, the higher-curvature arc electron energies can be found using $\beta = .16$ to be about 6.5 keV.

As in the case of the low curvature arcs, some of the higher-curvature arcs, cannot be explained by the model. Occasionally in the data set a series of arcs of higher curvature occur when the angle between the spacecraft and Io, $\phi \approx 180°$. For those cases (one good example is V1 day 79-34 at 12 - 16 hrs. [Fig. 12]) it is not possible to ray trace with the present O-4 magnetic field model, because an angle of $\phi \approx 180°$ would require the ray path to pass through Jupiter in order to be observed by the spacecraft. One possible way out of this dilemma is the introduction of a new B-field model such as the Smith et. al. (1975) D-4 model which might allow such ray paths. This is the case because the D-4 model has the geographic pole of Jupiter completely outside the Io-auroral oval, so that field lines with a foot on one hemisphere (for instance the north) might pass over the pole and above the opposite hemisphere. This would allow a source point located on one side of Jupiter at the foot of an Io flux tube to propagate to the opposite side of Jupiter from Io ($\phi \approx 180°$).

SUMMARY I

We have presented Jovian DAM ray-tracing results using the O-4 magnetic field model and a Jovian empirical-fit plasma model that includes the Io torus. The assumed emission mechanism requires that: (1) the radiation is R-X mode; (2) the source region is at the foot of an Io flux tube and the source mechanism is Doppler-shifted gyro-emission, and (3) the emission cone is hollow. The ray-tracing code is three-dimensional and based on the Stix cold-plasma formulation of the index of refraction and Haselgrove's set of first order differential equations.

We have shown that DAM ray paths refracted by the ambient plasma and local B-field can produce arc-like signatures as observed from the V1 and V2 spacecraft explained by intersecting the emission cones with the spacecraft trajectory. Because of the dependence of f_{R-X} on plasma and B-field parameters, a dispersion of frequencies occurs which duplicates the observed signatures in the data, in many, but not all, cases studied.

Our model arcs explain the vertex-early and vertex-late arcs of low curvature as due to very small Doppler-shifted gyro-emission emitted initially at constant wave normal angle, $\psi \approx 90°$, at all frequencies. There is good qualitative agreement for most of the low curvature arcs examined when the spacecraft is relatively far from Jupiter to minimize spacecraft motion effects. Some data does not match the model; however, as in cases where the model suggests no arcs should exist because the spacecraft-Io angle, ϕ, is much larger than 90°. For most examples of low-curvature arcs (cf. nested arcs of large frequency extent) the model successfully predicts the general shape and occurrence of the data examined. Decametric arcs of higher curvature seem to represent a different class of event.

In the data set one frequently observes either isolated or nested groups of arcs that have a larger curvature that cannot be explained if one assumes $\psi \approx$ constant $\approx 90°$. We have found one possible mechanism to adequately model this class of signature is to allow the wave normal to vary with frequency. This result yields a $\psi(f)$ relationship that seems to be typical of a large number of higher-curvature arcs. The $\psi(f)$ curve that typifies this class of arc is peaked around 10 MHz and falls off on either side with almost constant but different slopes the positive slope being somewhat larger than the negative slope. A semi-quantitative analysis of the $\psi(f)$ relationship based on the resonance condition (1), allows us to use the observed maximum value of ψ for the modeled higher-curvature arcs, $\psi_{max} \approx 76°$, to suggest $\beta \approx 0.16$. This value, based on the Doppler-shift expression (3) implies the maximum energy of higher-curvature arc-producing electrons is $\approx$6.5 keV, a reasonable value compared to suggested potential differences of several hundreds of kV across Io, a possible source of electron acceleration along the field lines (cf. Shawhan, 1976).

CONCLUSIONS I

We conclude from our results that many qualitative features of the DAM arcs are explained by assuming a gyro-emission mechanism along an Io flux tube. Resultant emissions are refracted by the ambient plasma and B-field to produce the arc-like signatures observed by Voyagers I and II. Both the shape and location of the data arcs examined are predicted. Our results imply that higher-curvature arcs may be due to more energetic electrons whose ultimate gyro-emission is more relativistically beamed to smaller wave normal angles. There are still unexplained observations. Our model has not yet explained some low-curvature emissions that occur for ϕ significantly different from 90° and some higher-curvature emissions for which $\phi \approx 180°$ (Io independent arcs). It may be necessary to incorporate a different B-field model such as the Smith et. al. D-4 model to explain the latter result, or invoke an electron source other than Io. The Warwick concept of B-field anomalies and/ or the Boischot model of arcs of the same frequency and source position producing an interference pattern cannot be ruled out for some arc events. We hope to resolve the discrepancies by future improvements of the model.

WHISTLER MODE RAY TRACING

The purpose of this study is to determine the maximum extent in latitude and in longitude of the Jovian high latitude lightning source region. From this, one can obtain a lower limit to the Jovian surface lightning density:

$$\text{lightning density} \approx \frac{\text{no. of strokes}}{\text{area}}$$

The ray tracing code is the same as described in the previous section--a 3-dimensional code based on the Haselgrove (1955) ray tracing equations and using the cold plasma index of refraction given by Stix (1962). The magnetic field model is that of Acuna and Ness (1976) with coefficients set to represent a dipole with a magnetic moment of 4.225 gauss R_j^3. The model of the magnetospheric plasma density is again the Sentman-Goertz plasma model (Sentman-Goertz, 1977). The Io plasma torus model was obtained by a spline fit interpolation of the density contours published by Warwick et al. (1979). This model is symmetric about the magnetic equator with a maximum density at the center of the torus of about 2500 cm^{-3} (Menietti & Gurnett, 1980). The total plasma density model used in the ray-tracing computer code is shown in Figure 3. The Jovian ionosphere used in this model is an empirical fit to the Voyager I ingress data published by Gehrels (1979) (Fig. 13). The maximum ionospheric density occurs at an altitude of approximately 2000 km. From the ray tracing code with the empirical ionospheric model included, the index of refraction at h ≈ 2000 km was found to be

$$n_{max} \approx 6.08 \quad .$$

Using Snell's law let us consider an atmospheric lightning burst refracting into the ionosphere and obtain limiting conditions.

Consider two points A and A' in the Jovian atmosphere which represent the maximum latitudinal extent of a lightning burst (Fig. 14). The distance between points A and A' represents the maximum extent of the lightning source region. For the limiting case consider a ray from point A to the south and tangent to the bottom of the ionosphere. Assuming the atmospheric index of refraction to be ≈ 1, we find, from Snell's law,

$$n_i \sin \Delta \approx 1$$

where n_i = the ionospheric index of refraction

Δ = angle between the wave normal vector and the normal to the surface at some point of the ray path (see Fig. 14).

For the limiting case, $n_i = n_{max}$

$$\Delta = \Delta_c ,$$

so

$$\sin \Delta_c = 1/6.08$$

$$\Delta = 9.47^\circ .$$

So rays from the atmosphere reaching the bottom of the ionosphere (C and C') with $\Delta > \Delta_c = 9.47^\circ$ will not reach the magnetosphere, but will be internally reflected. In a grossly exaggerated fashion Fig. 14 shows rays "1" and "2" from points A and A' respectively which both trace to point D in the Io torus. By ray tracing, we have found the points A and A' which will allow the ray paths of rays 1 and 2 to intersect at D in the Io torus.

In this study rays at a constant frequency of 3 kHz were launched from high Jovian latitude ($\approx 60^\circ$). For the latitudinal study the rays were launched in a meridian plane with the angle Δ (from Figure 14) fixed at 9.47°. It was assumed the satellite was located in the Io torus on the magnetic equator at $r = 6.0 R_J$. By trial and error it was found that rays launched from latitude = 58.6°, $\Delta = 9.47^\circ$, cross the magnetic equator at $r = 6.02\ R_J$ (corresponding to

ray 2 in Figure 14). Rays launched from latitude = 62.6°, Δ = 9.47°, cross the magnetic equator at r = 5.99 R_J (corresponding to ray 1 in Figure 14). The horizontal extent of points A and B is 4.0° and corresponds to a surface distance of about 4978 km. This is a large distance but represents the maximum extent detectable since we have taken the limiting case.

The longitudinal extent of the lightning source was investigated in a similar fashion. The ray source point was moved in longitude from a given reference lightning source longitude. Rays were launched at $\Delta \approx 9.47°$ while varying angle ψ, the angle between the wave normal vector and the magnetic field vector and varying β, the angle the wave normal makes relative to the meridian plane. By varying both the ray launch longitude and angle β while keeping $\Delta \lesssim 9.47°$ ray paths were found that crossed the magnetic equator at $r \approx 6.01\ R_J$. For larger excursions in longitude the ray path will not intersect the satellite position within the torus. So it is concluded that the maximum extent of the lightning source region in the longitudinal sense at this latitude is ~1.9°, corresponding to a horizontal distance of 2360 km. At latitude = 62.7° (the top of the latitudinal extent), longitude = ± .85° and β = 113°, rays cross the magnetic equator at r = 5.999 R_J. For larger excursions in longitude at this latitude the ray path will not intersect the satellite position within the torus. For this latitude the maximum longitudinal extent of the lightning source region is 1.7° corresponding to a horizontal distance of 1991 km. To reiterate, these are the maximum extents in longitude because we have considered the limiting case. If one crudely assumes a rectangle with maximum latitudinal extent of 4980 km and maximum longitudinal extent of 2400 km, the maximum area of detectable lightning source on the Jovian surface at high latitude is 1.2×10^7 km^2. Hence a lower limit to the lightning source density can be found if one knows the number of lightning strokes

occurring within this area. A summary of the latitude and longitude excursion computer runs is given in Table II.

TABLE II

Latitude Excursion Runs

Source Values					Magnetic Equator Crossing	
ψ	β	Δ	Latitude	Longitude	Radius	Longitude
26.4°	90°	-9.466°	58.6°	0°	$6.015R_J$	0°
5.06°	90°	+9.466°	62.6°	0°	$5.987R_J$	0°

Longitudinal Excursion Runs

Source Values					Magnetic Equator Crossing	
ψ	β	Δ	Latitude	Longitude	Radius	Longitude
26.4°	94°	-9.41°	58.6°	0.95°	$6.009R_J$	0°
5.0°	113°	9.86°	62.7°	0.89°	$5.9985R_J$	0°

In order to evaluate the wave energy dispersion, four rays were launched, each with a constant wave normal angle, ψ (either $\psi = 1°$, $\psi = 5°$, or $\psi = 10°$). Each ray was launched at a different angle β ($\beta = 0°$, 90°, 180°, 170°). The area intercepted by this envelope of rays at the top of the ionosphere and at the equator was measured. The rays' source points were the center of the latitudinal and longitudinal lightning source region determined above. The index of refraction and area at both points (a and b in Fig. 15) as well as the ratio of these two areas, A_2/A_1 are listed in Table III.

TABLE III

	ψ	Index of Refraction	Area (km^2)	A_2/A_1
A	1°	1.76	$A_1 = 6.7 \times 10^3$	3.9×10^3
B	1°	$47 < n < 53$	$A_2 = 2.6 \times 10^7$	
A	5°	1.76	$A_1 = 1.7 \times 10^5$	3.8×10^3
B	5°	$32 < n < 82$	$A_2 = 6.4 \times 10^8$	
A	10°	1.77	$A_1 = 7.3 \times 10^5$	3.8×10^3
B	10°	$51 < n < 96$	$A_2 = 2.8 \times 10^9$	

SUMMARY II

The whistler mode ray-tracing studies have demonstrated that by assuming a source point at high Jovian latitude and ray-tracing through the magnetosphere to the Io torus, an estimate of the lightning source extent on the Jovian surface can be made. This estimate is much smaller than that made by Lepping et. al (1981) who have performed the same study by starting at the Io torus and ray-tracing back toward the planet. This latter study achieved a surface area at least three times higher than ours. The discrepancy, we feel, is due to the high degree of wave refraction near the Jovian surface and consequent Landau damping effects which were not considered by Lepping et al. These damping effects are not as important for rays launched from the surface due to the higher phase velocity and smaller wave normal angle of the waves at the same point near the surface on the outbound trace compared to the inbound trace.

Our results can now be utilized to estimate the lightning source rate at Jupiter and, from the energy dispersion calculated, determine the approximate Jovian radio power output due to lightning bursts on the surface.

NEW IO TORUS MODEL

The Io torus contours presented by Warwick et. al. (1981) were a result of a first look at the Voyager 1 data. To draw the contours the assumption of torus symmetry with respect to the Jovigraphic equator was made. As a first approximation this is not a bad assumption; however, Hill et. al. (1974) have shown that the centrifugal equator is a much better assumed central axis of the Io torus. More recently, and post-Warwick Io torus model, Bagenal and Sullivan (1980) have presented a much more sophisticated look at the Io torus including the addition of ion contributions and both hot and cold species. The results of their work are shown in Figure 16 which depicts the Io torus electron density contours. This figure, when compared to Figure 1, immediately shows the effect of the hot electron species which are depicted as lobes or "horns" at approximately 5 R_J. Since the Bagenal-Sullivan model is a more accurate description of the torus it has been introduced into our new ray-tracing code.

To reproduce the results of Bagenal and Sullivan linear interpolation of table values are made numerically in two dimensions: along the radial direction and along the magnetic field line. The table values present electron density along the magnetic field line as a function of L-shell. A grid of points is represented between radial distances of 5 and 8.5 R_J and up to 1.5 R_J above the centrifugal equator at 0.1 R_J intervals. The points in the grid have been put on the meridional plane where the magnetic and rotational equators are aligned ($\lambda_{III} \approx 291°$) so that the plasma is symmetrically distributed about these equators. Azimuthal symmetry is also assumed.

An Euler transformation allows us to transform from Jovigraphic coordinates to Jovian magnetic coordintes which are tilted with respect to the

latter by the complement of the angle, α, shown in Figure 17. It is a three-dimensional transformation, so that any longitude can be chosen. The angle γ in Figure 17 can be shown for a dipole field to be

$$\gamma = \tan^{-1} \{2/3 \tan \alpha/(1 + \sqrt{1 + 8/9 \tan^2 \alpha})\} \qquad (1)$$

The arc length along the magnetic field line can be shown to be

$$S = -\frac{\sqrt{3}}{2} \frac{r}{(1-u^2)} \{u \sqrt{\frac{1}{3} + u^2} + \frac{1}{3}\ln(u + \sqrt{\frac{1}{3} + u^2}) - \frac{1}{3}\ln \sqrt{\frac{1}{3}}\} \qquad (2)$$

where $u = \cos\theta$.

The numerical number density can then be found by evaluating $\partial n/\partial r$ and $\partial n/\partial \theta$, where the derivatives can be evaluated directly from table values after first noting that

$$\partial n/\partial \theta = (\partial n/\partial s)\ (\partial s/\partial \theta)$$

and $\partial s/\partial \theta$ is evaluated from (2) above.

SUMMARY III

The Bagenal-Sullivan torus has been incorporated into the new ray-tracing code, and will provide a much better basis for the ray-tracing of low frequency radiation in the Io torus.

REFERENCES

Acuna, Mario H., and N. F. Ness, "The Main Magnetic Field of Jupiter", J. Geophys. Res. 81, 2917, 1976.

Bagenal, F. and J. D. Sullivan, "Direct Plasma Measurements in the Io Torus and Inner Magnetosphere of Jupiter", J. Geophys Res., 86, 8447, 1981.

Boischot, A. and M. G. Aubier, "The Jovian Decametric Arcs as an Interference Pattern", J. Geophys. Res., 86, 8561, 1981.

Boischot, A., A. Lecacheux, M. L. Kaiser, M. D. Desch, J. K. Alexander, and J. W. Warwick, "Radio Jupiter after Voyager: An Overview of the Planetary Radio Astronomy Observations", J. Geophys. Res., 86, 8213, 1981.

Calvert, W., "The Auroral Plasma Cavity", Geophys. Res. Letts., 8, 919, 1981.

Carr, T. D. and S. Gulkis, "The Magnetosphere of Jupiter", Ann. Rev. Astron. Astrophys., 7, 577, 1969.

Gehrels, T., Ed., Jupiter, (Univ. of Arizona Press, Tucson, 1976).

Goertz, C. K., "Io's Interaction with the Plasma Torus", J. Geophys. Res., 85, 2949, 1980.

Goldreich, P. and D. Lynden-Bell, "Io, a Jovian Unipolar Inductor", Astrophys. J., 156, 59, 1969.

Gurnett, D. A., and C. K. Goertz, "Multiple Alfven Wave Reflections Excited by Io: Origin of the Jovian Decametric Arcs", J. Geophys. Res., 86, 717, 1981.

Hashimoto, K., and M. L. Goldstein, "A Theory of the Io Phase Assymetry of the Jovian Decametric Radiation", NASA Technical Memorandum 83994, Aug., 1982.

Hill, T. W., A. J. Dessler and F. C. Michel, "Configuration of the Jovian Magnetosphere", Geophys. Res. Letts., 1, 3, 1974.

Melrose, D. B., "An Interpretation of Jupiter's Decametric Radiation and the Terrestial Kilometric Radiation as Direct Amplified Gyro-emission", Astrophys. J., 207, 651, 1976.

Menietti, J. D. and D. A. Gurnett, "Whistler Propagation in the Jovian Magnetosphere", Geophys. Res. Letts., 7, 49, 1980.

Neubauer, F. M., "Nonlinear Standing Alfven Wave Current System at Io: Theory", J. Geophys. Res., 85, 1171, 1980.

Omidi, N. and D. A. Gurnett, "Growth Rate Calculations of Auroral Kilometric Radiation using the Relativistic Resonance Condition", J. Geophys. Res., 87, 2377, 1982.

Shawhan, S. D., "VLF Ray Tracing in a Model Ionosphere", Res. Rep. 66-33, Dept. of Physics and Astronomy, Univ. of Iowa, 1966.

Shawhan, S. D., "Io Sheath-Accelerated Electrons and Ions", J. Geophys. Res., 81, 3373, 1976.

Smith, E. J., L. Davis, Jr., D. E. Jones, P. J. Coleman, Jr., D. S. Colburn, P. Dyal, and C. P. Sonett, "Jupiter's Magnetic Field, Magnetosphere, and Interaction with the Solar Wind: Pioneer 11", Science, 188, 451, 1975.

Stix, T. H., The Theory of Plasma Waves, McGraw-Hill Book Co., Inc., 5-34, 1962.

Warwick, J. W., J. B. Pearce, A. C. Riddle, J. K. Alexander, M. D. Desch, M. L. Kaiser, J. R. Thieman, T. D. Carr, A. Boischot, C. C. Harvey, and B. M. Pederson, "Voyager I Planetary Radio Astronomy Observations Near Jupiter", Science, 204, 995, 1979.

Wu, C. S. and L. C. Lee, "A Theory of the Terrestrial Kilometric Radiation", Astrophys. J., 230, 621, 1979.

FIGURE CAPTIONS

Figure 1. A large isolated arc double-valued in frequency is seen beginning at about 1155 UT at both high and low frequencies with a vertex at about 1235 UT.

Figure 2. Frequency versus time spectrogram for V1-79-63 depicting a series of low curvature nested arcs especially clear between about 950 UT and 1030 UT.

Figure 3. Model Jovian Magnetosphere. Contours of Plasma frequency are from Sentman and Goertz (1978), B-field from Acuna and Ness (1976), Io torus from Warwick, et al (1979).

Figure 4. Calculated Radiation Sheets for Two Northern Hemisphere Sources: 2 MHz and 20 MHz, and for Two Southern Hemisphere Sources: 2 MHz and 10 MHz. The radial shell at six Jupiter radii ($6R_J$) is shown in mercator projection. The source points are designated by "X" and all rays are launched at 90° with respect to the B-field. The Io torus is shown in longitudinal cross section, shaded.

Figure 5. Calculated Emission Cones for the Same Source Points as in Fig. 4., but now Intersecting the $100R_J$ Radial Shell.

Figure 6. Calculated Emission Cones for Wave Normal Angles (WNA's) of 60°, 80°, 100°, and 120°. The mercator projection is taken at $100R_J$, top panel: 2MHz, bottom panel: 25 MHz.

Figure 7. Calculated Emission Cones Emanating from Sources Located at Different Longitudes. All rays have been launched at 90°, wave frequency 25 MHz, mercator projection at $100R_J$.

Figure 8. Frequency versus system III'65 Longitude. The points designated by squares are model points. The numbers above the model curves depict the approximate Io flux tube longitude chosen for the source points. The event on the left is V2-79-197; the right event is V2-79-182.

Figure 9. Frequency versus system III'65 Longitude showing the model arcs for each 10° interval of longitude. The Io longitude is labelled on each arc. The wave normal angle at the source point for all these arcs was 90°.

Figure 10. High Curvature Arcs, Double-Valued in Frequency, are shown here for V1-79-71 (left) and V2-79-188. These arcs are fairly typical of high curvature arcs and were chosen because of their isolated nature making them easier to measure.

Figure 11. Wave Normal Angle, ϕ, versus frequency found empirically by varying ϕ until the model arcs matched the observed arcs for V1--79-72 (top) and V2-79-188 (bottom).

Figure 12. Frequency versus time spectrogram for V1-79-34. Several arcs occur between 1347 UT and 1527 UT while the angle, ϕ, between the spacecraft and Io is approximately 180°.

Figure 13. Altitude versus Electron Number Density for the Jovian Ionosphere as Determined during Voyager 1 Ingress and Published by Gehrels (1979).

Figure 14. A Schematic Diagram of Whistler Ray Paths "1" and "2" from Points A and A' Respectively which Both Trace to Point D in the Io torus. The points A and A' represent the maximum latitudinal extent of a lightning burst on the surface of Jupiter. "N" is the normal to the surface at A and A'. C and C' designate the bottom of the ionosphere; Δ is the angle between the wave normal vector and the normal to the surface at some point of the ray path.

Figure 15. A Schematic Diagram Depicting the Ray "Cone" Produced by Four Whistler Waves Stimulated by Lightning in the Center of the Jovian Lightning Source Region (as defined in the text). The dispersion of this ray cone is crudely found by comparing the area A, at point "a", the top of the ionosphere, to the area A_2 at point "b", the magnetic equator.

Figure 16. Density Contours of the Io Torus as Published by Bagenal and Sullivan (1981). The vertical axis is a measure of the distance above the centrifugal equator (as defined in the text). The dashed lines depict the inbound and outbound trajectories of V1.

Figure 17. A Schematic Diagram showing the Jovicentric Angular Velocity, $\bar{\omega}$, tilted with respect to the magnetic moment vector, $\bar{m}$, by the compliment of the angle α. The angle γ is between the centrifugal equator and the magnetic equator. The arc length, s, is along the (dotted) dipole magnetic field line between some reference point at angle θ and the magnetic equator. The actual field lines (solid) are shown distorted by the centrifugal plasma pressure.

ACKNOWLEDGEMENTS

We would like to thank the GSFC radio astronomy group for supplying us with Voyager I and II PRA data. We would also like to thank Jerome De La Cruz for his assistance in programming. This work was supported by NASA contract NAS7-100 through Cal Tech/JPL Contract 956026.

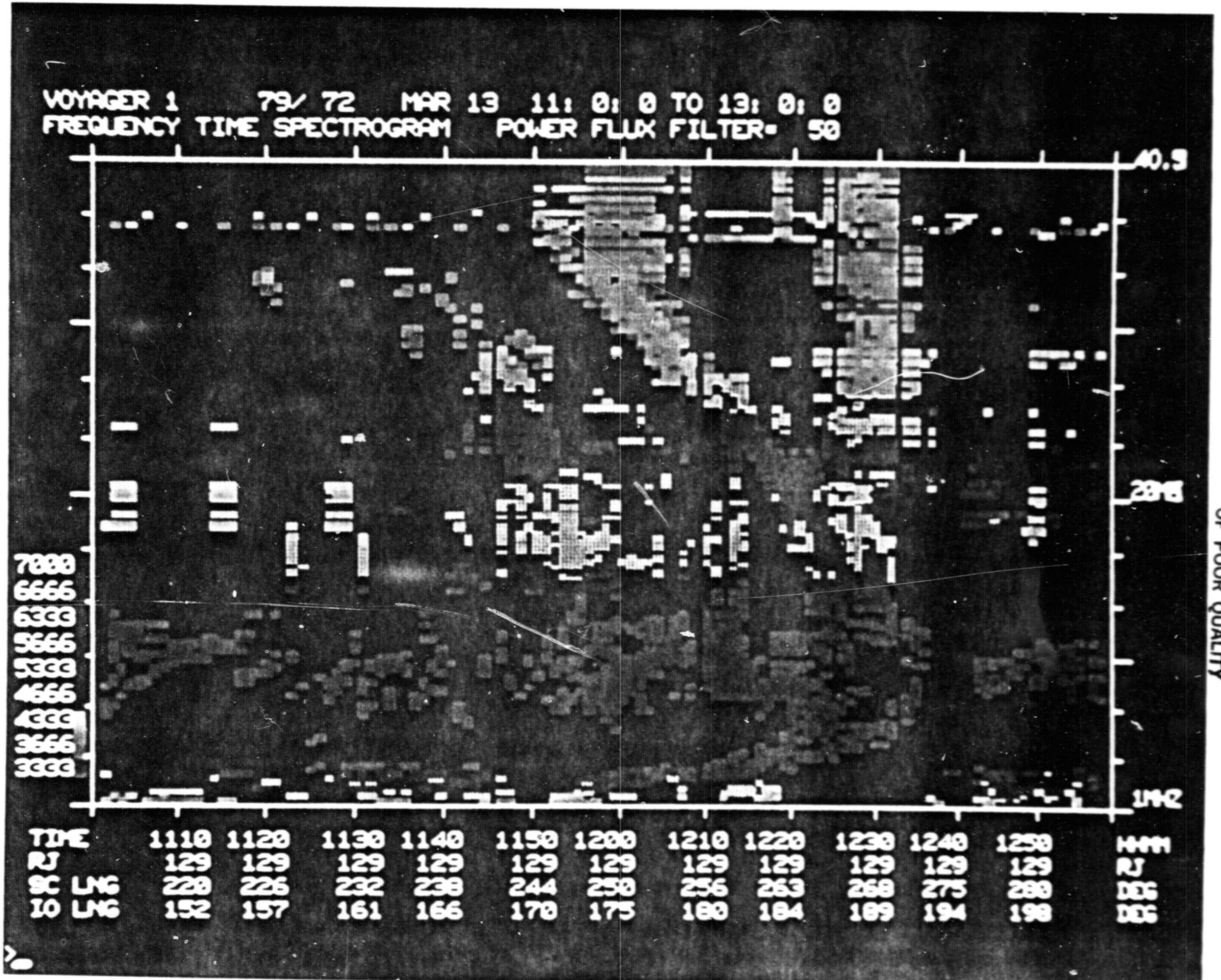

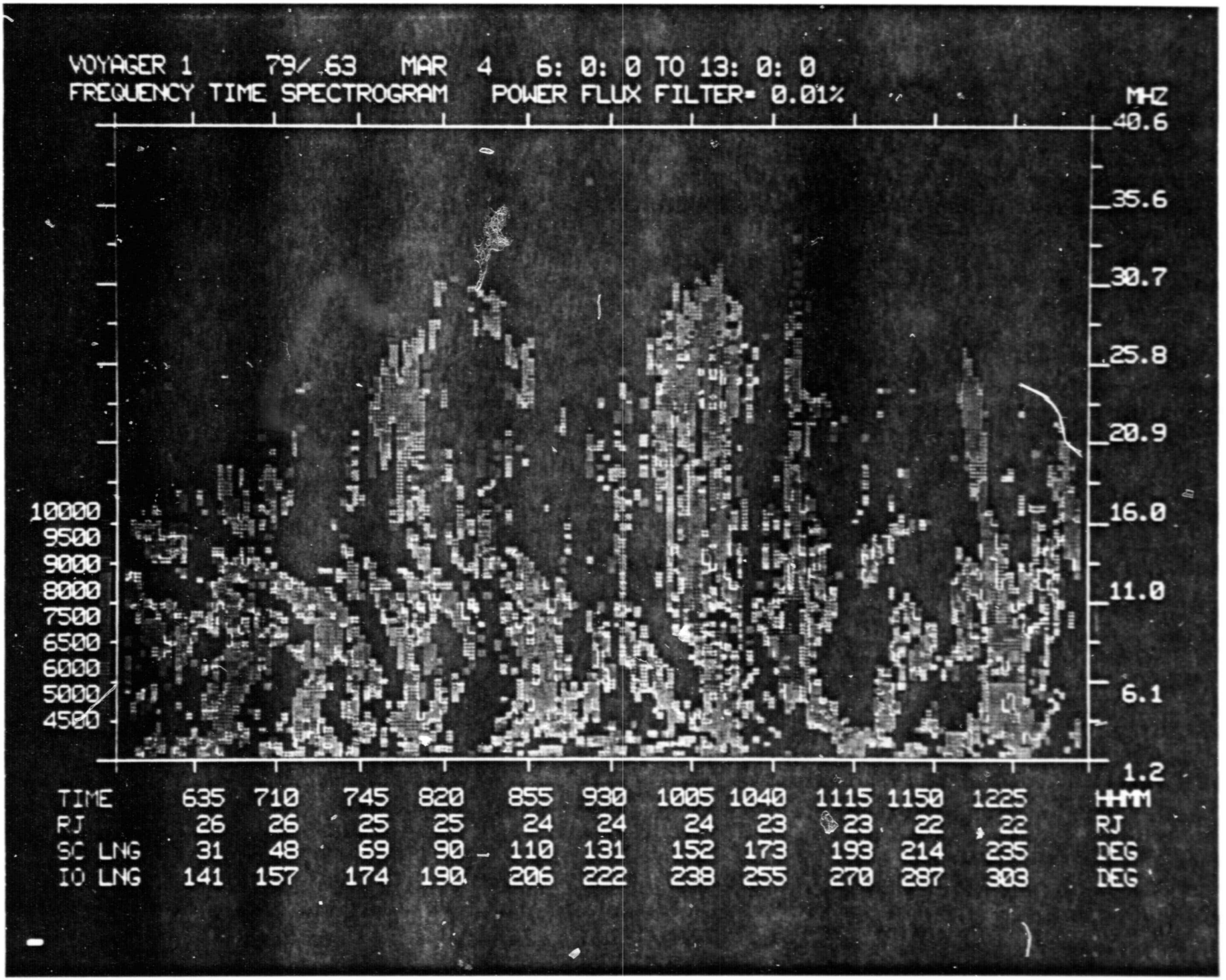

CONTOURS OF Fp (KHz)

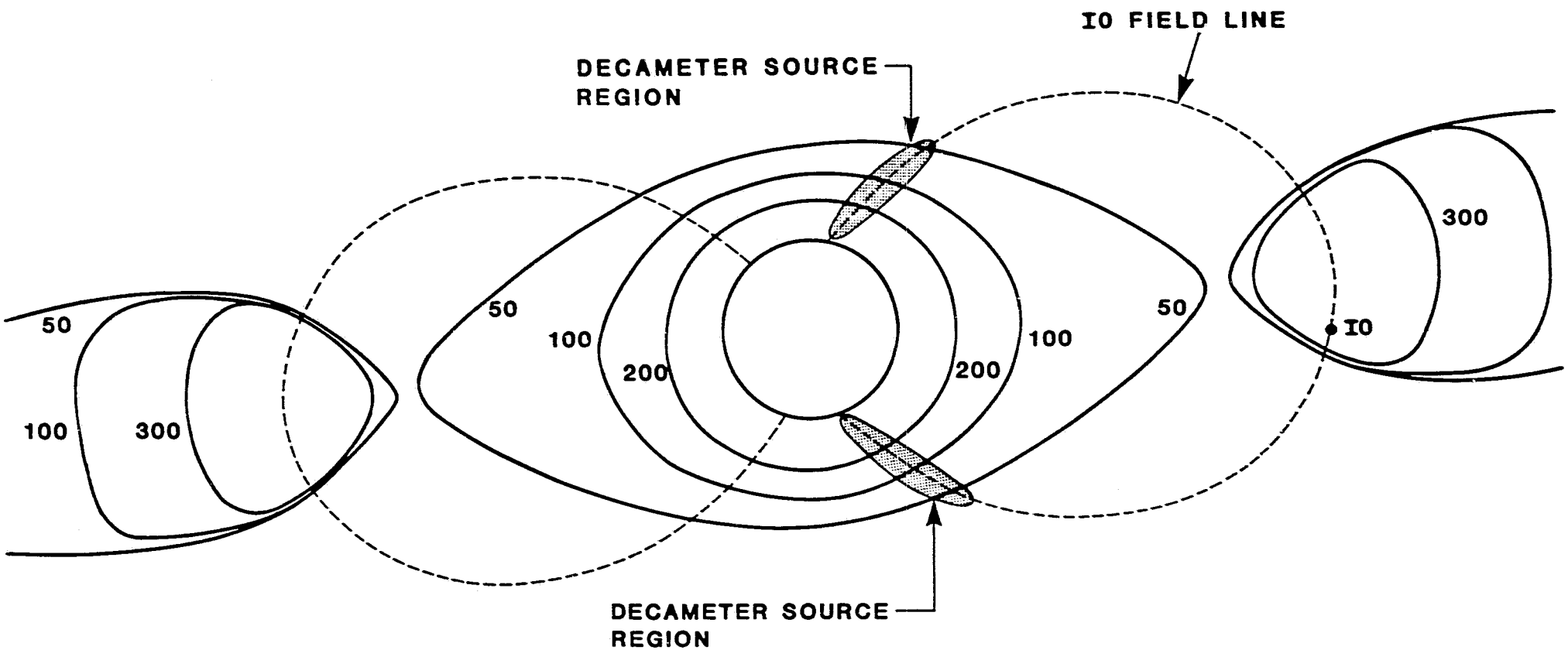

SYSTEM III LONGITUDE = 200°

SYSTEM III LONGITUDE = 20°

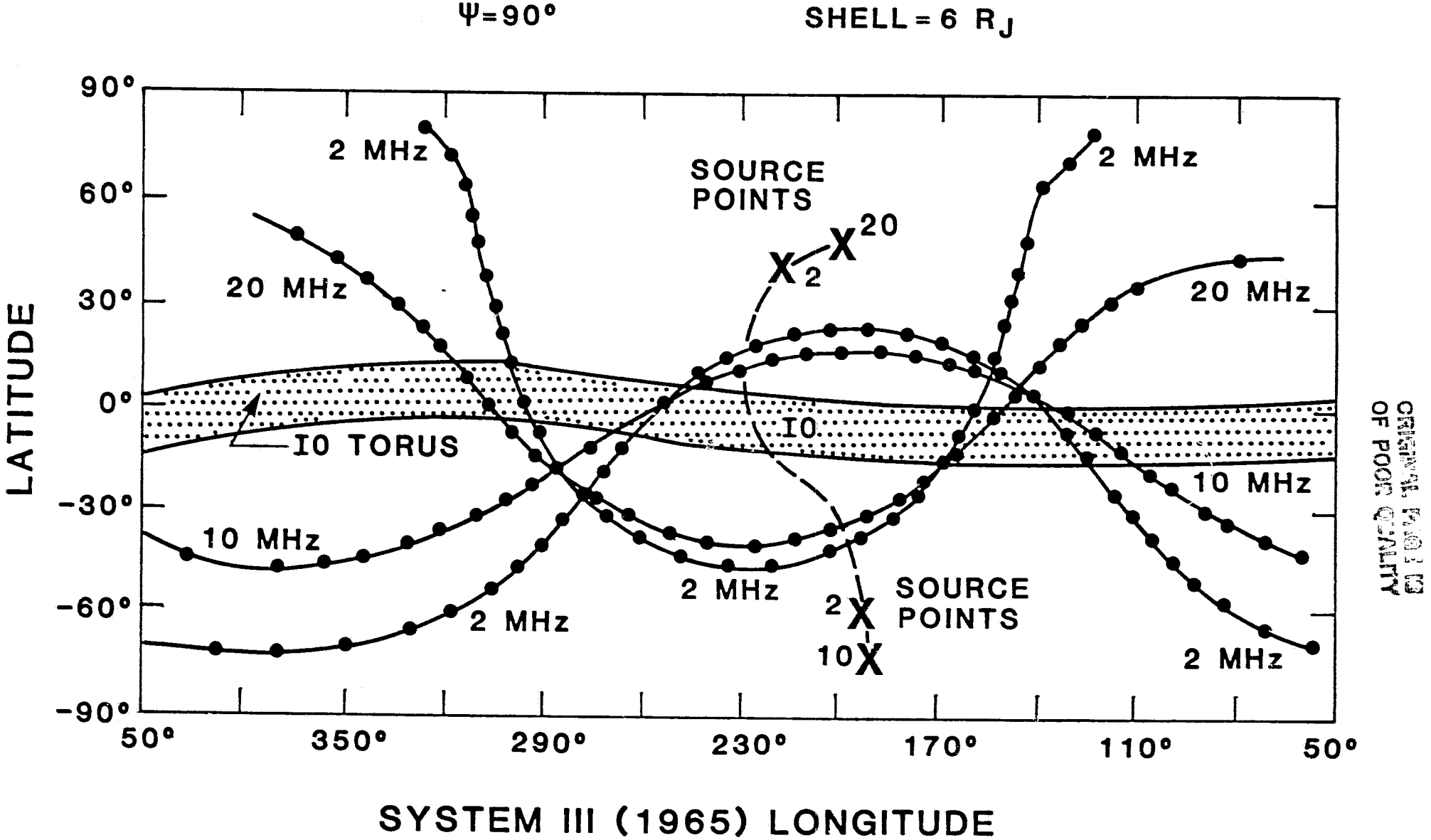

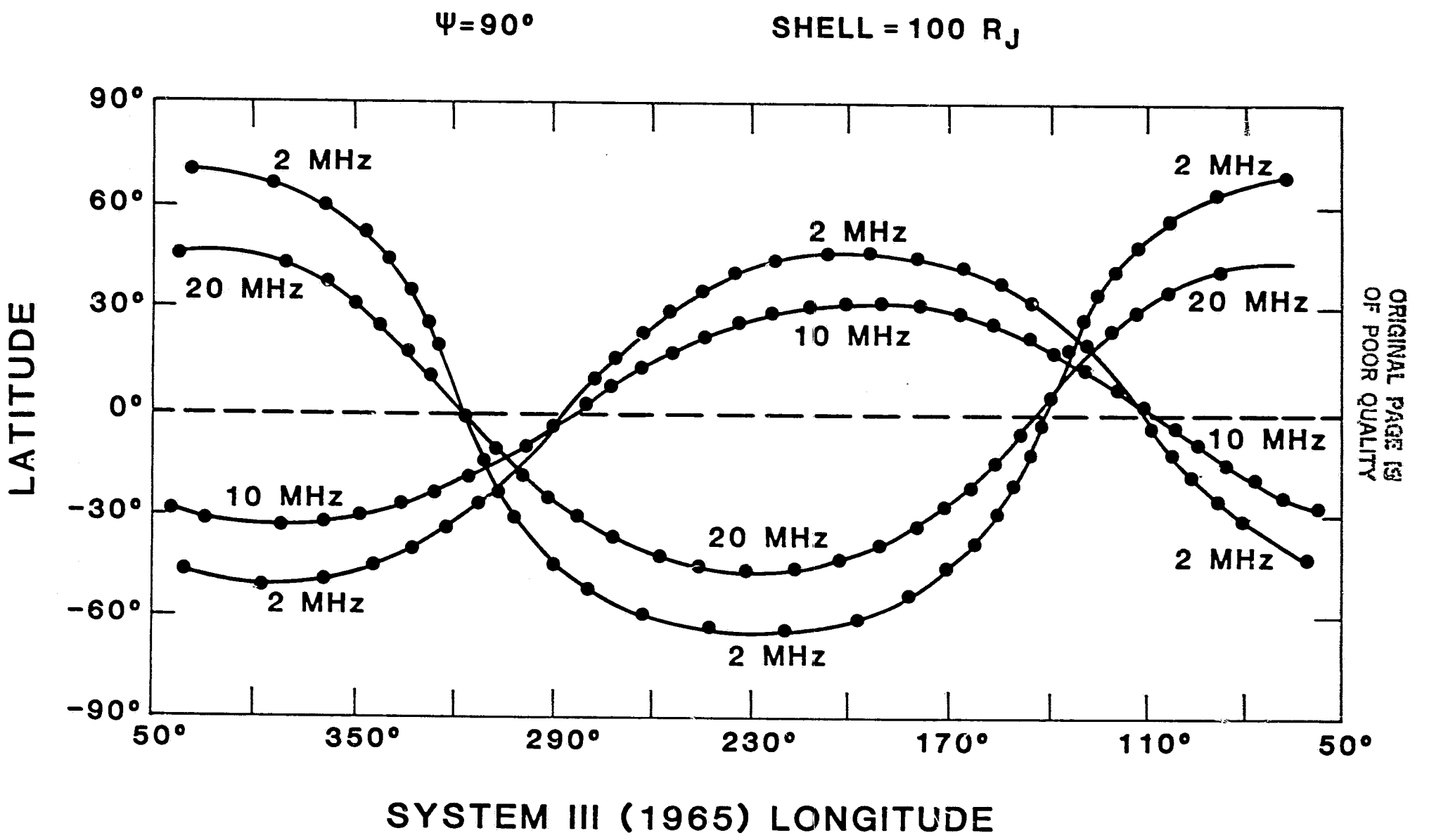
Ψ=90°
SHELL = 100 R_J
90°
60°
30°
0°
-30°
-60°
-90°
LATITUDE
2 MHz
20 MHz
10 MHz
2 MHz
20 MHz
10 MHz
2 MHz
2 MHz
20 MHz
10 MHz
2 MHz
2 MHz
50°
350°
290°
230°
170°
110°
50°
SYSTEM III (1965) LONGITUDE
ORIGINAL PAGE IS
OF POOR QUALITY

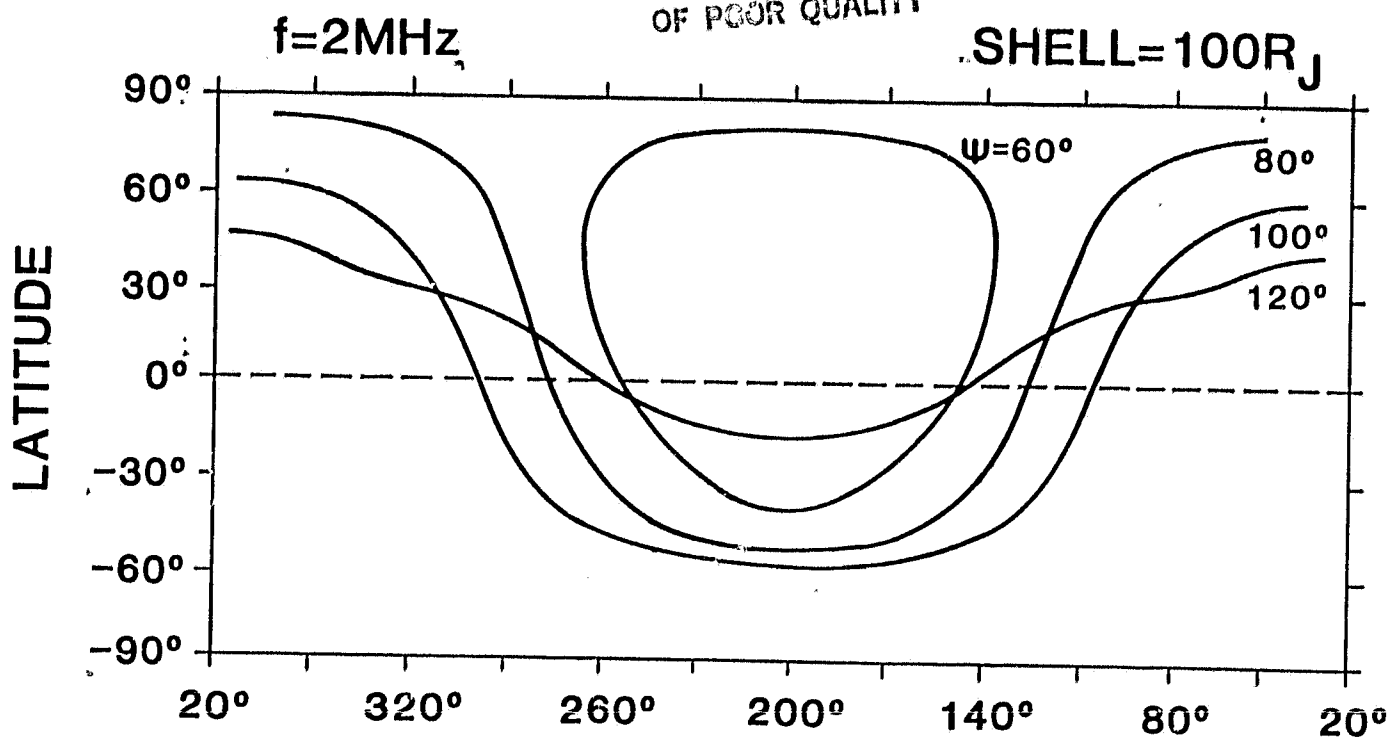

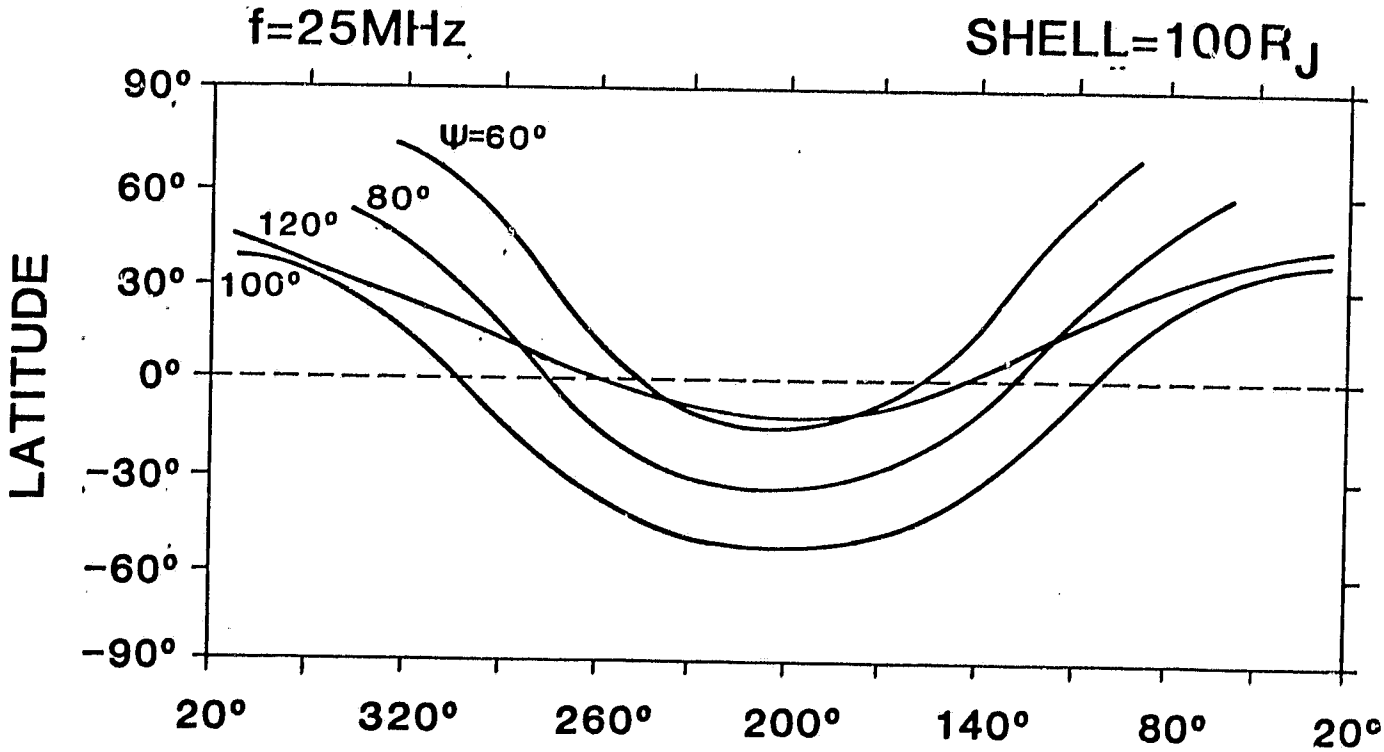

FREQUENCY = 25MHz SHELL = 100R_J Ψ=90°